Suppressing Two-Plasmon Decay with Laser Frequency Detuning

In direct-drive inertial confinement fusion (ICF), a cryogenic capsule of deuterium–tritium fuel with a thin outer ablator material is imploded by direct laser illumination.[1,2] An efficient implosion maximizes the amount of laser energy that is converted into kinetic energy of the imploding shell while minimizing the premature heating of the cold fuel by hot-electron preheat.[3] Preheat reduces the implosion efficiency by decreasing the compressibility of the capsule. Radiation–hydrodynamic simulations suggest that converting as little as 0.1% of the incident laser energy into preheat can significantly degrade implosion performance.[4]

The dominant source of hot electrons in direct-drive ICF experiments on the OMEGA laser[5] is the two-plasmon–decay (TPD) instability.[6] Two-plasmon decay occurs when an incident light wave decays into two electron plasma waves (EPW's) at near-quarter-critical densities.[7–10] When the driven EPW's become large in amplitude, the instability undergoes nonlinear saturation, resulting in a broad spectrum of EPW's[11,12] that can stochastically accelerate electrons to energies >100 keV (Ref. 13). The fraction of incident laser energy converted into hot electrons (f_{hot}) has been observed to exceed 1% at ignition-relevant laser intensities,[14] and experiments indicate that ~25% of the hot-electron energy is coupled to the cold fuel.[15] This suggests that hot-electron preheat is close to or above tolerable levels in the highest-intensity OMEGA experiments.

TPD-driven preheat currently limits the peak laser intensity in direct-drive ICF implosions to $\sim 10^{15}$ W/cm^2. A number of studies have shown that alternative ablator materials can be used to mitigate TPD,[16,17] but this approach allows for only modest increases in laser intensity and precludes the optimization of the ablator for hydrodynamic efficiency.

The main reason that TPD is a limiting instability for direct-drive ICF is that many overlapping laser beams can drive the instability cooperatively.[18] This results in hot electrons being observed even when the single-beam laser intensities are well below the instability threshold. The requirement of spatial coherence of the cooperating beams restricts them to lie on a cone in the homogeneous theory,[19,20] but the short spatial extent of the TPD interaction region in inhomogeneous plasmas allows for a cooperative interaction between laser beams with a correspondingly short coherence length.[21] The cooperative nature of the instability, however, also provides a unique path to TPD suppression by decoupling the multibeam instability.

In this article we present computer simulations that indicate that frequency detuning of the drive laser beams can suppress the TPD instability and corresponding hot-electron generation in direct-drive ICF using existing lasers. Three-dimensional simulations using realistic plasma conditions and the laser configuration for an OMEGA implosion indicate that frequency detuning of $\Delta\omega/\omega_0 \sim 0.7\%$ (1.76 nm) is sufficient to decouple a pair of laser beams, effectively doubling the intensity threshold for the onset of hot-electron generation. The simulations show that suppression of the absolute instability[9] is sufficient to eliminate TPD-driven hot-electron production, and that 0.7% frequency detuning would be more than enough to eliminate TPD-driven hot-electron production in OMEGA experiments. Further increases in the available detuning would allow the laser to be divided into more distinct frequencies, which can further increase the instability threshold and open up the ICF design space. This result is in contrast to using continuous-bandwidth lasers where the same reduction in hot electrons would require at least as much bandwidth, which is not achievable with current ICF laser systems.

It was recognized in early studies that temporal incoherence in the form of laser bandwidth could be used to suppress laser–plasma instabilities,[22,23] but the large-scale glass lasers that are currently used to conduct ICF experiments are nearly monochromatic ($\delta\omega/\omega_0 < 0.1\%$, where $\delta\omega$ is the laser bandwidth). Frequency detuning (i.e., introduction of multiple discrete frequencies) of a fraction of the laser beams has been used to control symmetry in indirect-drive ICF experiments[24] and to mitigate cross-beam energy transfer in polar-direct-drive experiments at the National Ignition Facility (NIF).[25] This technique was generally not expected to be useful for TPD suppression at the modest frequency shifts that are currently available. Early

work showed that the homogeneous temporal growth rate (γ_0) could be reduced by a factor of $\gamma_0/\delta\omega$ when $\delta\omega \gg \gamma_0$ (Refs. 22, 26, and 27). The homogeneous growth rate for TPD can easily be ~1% of the laser frequency for ICF conditions, which suggests $\delta\omega/\omega_0 \gg 1\%$ is required to have a significant impact on TPD.[28,29] In an inhomogeneous plasma, however, these results are only directly applicable to instabilities that saturate convectively (i.e., undergo finite spatial amplification) because the convective gain is directly related to the linear growth rate. Two-plasmon decay becomes absolutely unstable (temporal growth at a fixed point in space) when the convective gain is relatively small ($\lesssim 2\pi$) (Ref. 30). The linear growth rate plays a reduced role in absolute instabilities because they always grow until saturated by some nonlinear mechanism.

Two-plasmon–decay simulations were performed using the *LPSE* (laser-plasma simulation environment) code.[11] The *LPSE* modules used in this study were the pseudospectral solver[31] for the extended Zakharov equations for TPD[32] and the hybrid particle evolution (HPE) module.[21] *LPSE* has had considerable success in reproducing previous experimental results, including measured plasma wave amplitudes[11] and hot-electron generation,[21] which suggests that the simulation results give a quantitative representation of what would be observed in experiments.

The 3-D *LPSE* simulations were performed in a $67.5 \times 13 \times 13$-μm^3 region on a $1688 \times 324 \times 324$-cell Cartesian grid. There was a linearly varying density along the x direction from $n_e/n_c = 0.19$ to 0.27, where n_e is the electron density and n_c is the critical density for the 351-nm drive beams. This gives a scale length of $L_n = 211$ μm at $n_c/4$. A plastic (CH) plasma was used with an electron (ion) temperature of $T_e = 2.6$ keV ($T_i = 1.0$ keV) and a Mach 1.2 flow antiparallel to the density gradient. These plasma conditions were determined from radiation–hydrodynamic simulations of an OMEGA implosion using the code *LILAC*.[33] Because the results are sensitive to the relative phase of the drive beams, all of the *LPSE* results correspond to the mean and standard deviation of five-run ensembles with random polarizations, phases, and speckle patterns.

Figure 153.33 shows the absolute instability thresholds from 3-D *LPSE* simulations that were designed to emulate the quarter-critical conditions in an OMEGA implosion near the time of peak hot-electron production. The overlapped laser intensities are normalized to the analytic result for the absolute threshold of a monochromatic plane wave $I_{Simon} = 233\, T_e/L_n$ in units of 10^{14} W/cm^2 (Ref. 9). A single OMEGA "hex" was simulated consisting of six laser beams incident from the corners of a hexagon, each with an angle of 23° relative to the density gradient (Fig. 153.34). The beams were simulated with phase plates and polarization smoothing, as described in Ref. 11. The simulations were performed with two or three laser frequencies, and two different methods were used to split the beams into multiple frequencies: (1) "multicolor," where each beam was split into N_ω frequencies with each frequency component containing $1/N_\omega$ of the laser energy, and (2) "tiled,"

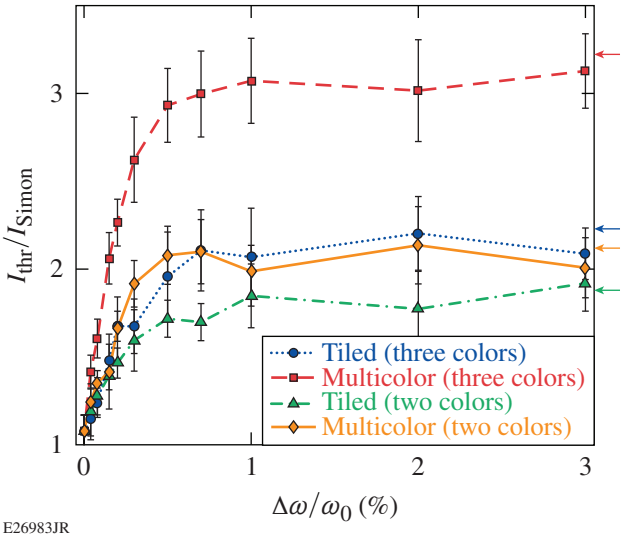

Figure 153.33
LPSE-simulated absolute two-plasmon–decay (TPD) thresholds for various types of frequency detuning. The curves correspond to three-color multicolor (red squares) and tiled (blues circles) detuning and two-color multicolor (orange diamonds) and tiled (green triangles) detuning. The arrows at the right edge indicate the expected asymptotic thresholds.

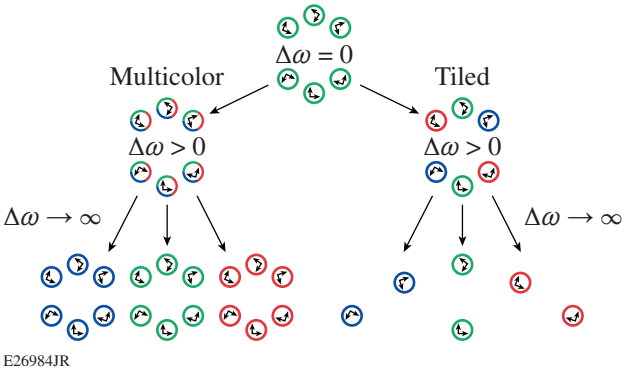

Figure 153.34
Schematic of the effect of three-color multicolor and tiled frequency detuning. The arrows correspond to one realization of random polarization with polarization smoothing. The third row corresponds to the three effective interactions occurring at different densities when the three frequencies are fully decoupled; the absolute threshold is three times the minimum threshold.

where each beam is monochromatic, but the different beams have different frequencies (alternating around the corners of the hexagon). In all cases, $\Delta\omega/\omega_0 \approx 0.7\%$ was sufficient to reach the asymptotic ($\Delta\omega \to \infty$) threshold ($\Delta\omega$ is the nearest-neighbor frequency separation).

Despite the multicolor approach being superior from the point of view of TPD suppression because of the higher instability thresholds, the tiled approach is included here because it is an easier laser architecture to implement and resembles what is currently available on large-scale laser facilities. For instance, the NIF[34] uses a tiled laser architecture that currently has $\Delta\omega/\omega_0 \approx 0.15\%$ with $\Delta\omega/\omega_0 = 0.35\%$ achievable with minor modifications. One of the OMEGA EP[35] beams has recently been upgraded to have $\Delta\omega/\omega_0 \approx 1\%$.

Figure 153.34 illustrates why the multicolor and tiled approaches to frequency detuning give different instability thresholds in the asymptotic limit of large $\Delta\omega/\omega_0$. In both cases the distinct frequencies decouple in the asymptotic limit, but in the multicolor approach, the threshold is simply N_ω times the threshold for $\Delta\omega = 0$ because the decoupling effectively results in N_ω six-beam interactions that are identical to the six-beam interaction at zero frequency detuning. When the individual beams have different frequencies, there are only $6/N_\omega$ beams in each of the N_ω groups of decoupled monochromatic beams. In this case, the effective decoupled configurations are not equivalent to the original six-beam configuration. For random polarizations, the different groups of decoupled beams will have different thresholds, and the overall threshold for the configuration to be absolutely unstable will be N_ω times the minimum threshold for the $6/N_\omega$ different groups. This qualitative picture suggests an alternative way to calculate the asymptotic thresholds in the tiled configuration: run N_ω monochromatic simulations with $6/N_\omega$ beams (random polarizations) and take N_ω times the minimum threshold as the expected asymptotic threshold. Repeating this procedure for an ensemble of five realizations of polarization and phase gives asymptotic thresholds of 2.27 ± 0.30 for $N_\omega = 3$ and 1.84 ± 0.12 for $N_\omega = 2$, which are in agreement with the corresponding results in Fig. 153.33 (2.09 ± 0.15 for $N_\omega = 3$ and 1.92 ± 0.16 for $N_\omega = 2$).

In the ICF context, the figure of merit for TPD mitigation is reducing hot-electron production. A commonly used semi-empirical metric for the onset of hot-electron production in multibeam experiments is the single-beam absolute threshold evaluated at the overlapped laser intensity. For this to be a useful metric, the following pair of conditions must be met: (1) the onset of hot-electron production corresponding to absolute instability, and (2) a multibeam absolute threshold identical to the single-beam threshold (using overlapped laser intensity). The first condition is true because the absolute threshold occurs when the convective gains are modest, so the convectively saturated waves are not large enough to generate significant hot electrons. It is not obvious that the second condition should hold for multiple beams with phase plates, polarization smoothing, and random relative polarizations, but note that in Fig. 153.33, the threshold at zero detuning is relatively close to the single-beam threshold. This behavior results from a combination of three effects: (1) the six beams act cooperatively to drive a common wave; (2) the random relative polarizations/phases of the beams tend to increase the threshold intensity; and (3) the phase plates cause the beams to have localized hot spots that effectively reduce the threshold.

Figure 153.35 shows the fraction of incident laser energy converted into hot electrons (>50 keV) in six-beam, three-color *LPSE* simulations. Two laser intensities were used: 4×10^{14} W/cm^2 and 7×10^{14} W/cm^2, which correspond to $I_{\text{thr}}/I_{\text{Simon}} = 1.63$ and 2.86, respectively. At $I = 4 \times 10^{14}$ W/cm^2, only ~0.1% frequency detuning was required to eliminate hot-electron production in the multicolor configuration, whereas ~0.3% was required in the tiled configuration. At $I = 7 \times 10^{14}$ W/cm^2, ~0.7% detuning was

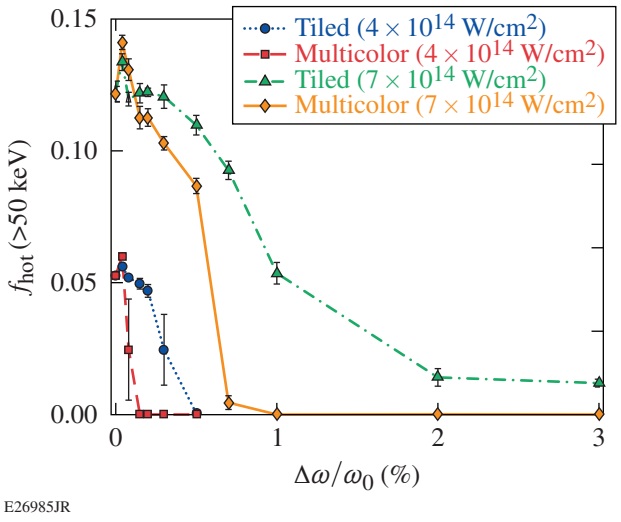

Figure 153.35
LPSE-simulated fraction of incident laser energy converted into hot electrons with energy >50 keV using OMEGA plasma conditions and three-color beams. The four curves correspond to the tiled (blue circles) and multicolor (red squares) configurations at $I = 4 \times 10^{14}$ W/cm^2 and the tiled (green triangles) and multicolor (orange diamonds) configurations at $I = 7 \times 10^{14}$ W/cm^2. The hot-electron production was taken as the average over 5 ps after the simulations reached a quasi steady state (12 ps).

required in the multicolor configuration, and no amount of detuning was sufficient to completely suppress hot-electron production in the tiled configuration because some of the frequency-matched beam pairs were still above the absolute threshold, even when the various colors were completely decoupled. This is consistent with the results shown in Fig. 153.33, where $I_{\rm thr}/I_{\rm Simon}$ never gets above 2.86 in the three-color tiled configuration, which is required to suppress the absolute instability at $I = 7 \times 10^{14}$ W/cm^2.

Note that the laser intensities used in Fig. 153.35 correspond to the overlapped intensity at the quarter-critical surface. The quoted laser intensity for an ICF implosion design typically corresponds to the peak laser power divided by the surface area of the undriven target, which is about 3× the intensity at $n_c/4$ in OMEGA implosions. The simulations at 4×10^{14} W/cm^2 correspond to the peak laser intensities that are currently available on OMEGA. The hot-electron fractions shown in Fig. 153.35 are a few times higher than what is observed in OMEGA implosions because they correspond to instantaneous rather than time-averaged hot-electron production.

To show the physical behavior in the simplest possible configuration, 2-D *LPSE* simulations were performed using normally incident plane waves. The grid and plasma conditions in the 2-D simulations were identical to the 3-D simulations along the x and y dimensions except that the EPW damping and flow were turned off. Figure 153.36 shows the absolute instability thresholds from *LPSE* simulations of two to five p-polarized, collinear plane-wave beams with electric field (enveloped at ω_0)

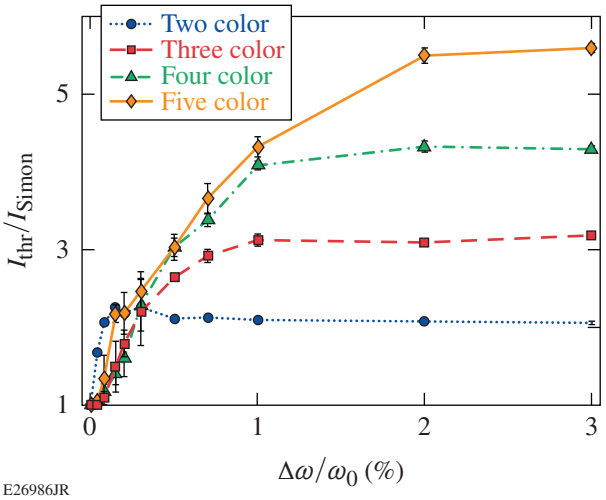

Figure 153.36
Absolute instability thresholds from 2-D *LPSE* simulations of collinear, plane-wave beams using two (blue circles), three (red squares), four (green triangles), and five (orange diamonds) colors.

$$\mathbf{E}_0 = \hat{y}\,\frac{E_0}{2}\sum_{j=1}^{N_\omega} e^{\,i(k_j x - \Delta\omega_j t + \phi_j)} + \text{c.c.},$$

where ϕ_j is the initial phase of the jth beam,

$$\Delta\omega_j = \left[j - (N_\omega + 1)/2\right]\Delta\omega$$

is the frequency shift,

$$k_j = \left(\omega_0/c\right)\sqrt{\left(1 + \Delta\omega_j/\omega_0\right)^2 - n_e/n_c},$$

and in cgs units $E_0 = \sqrt{8\pi I \big/ \left[c\left(1 - n_e/n_c\right)^{1/2}\right]}$ (note that the maximum frequency separation increases with increasing N_ω because $\Delta\omega$ is defined as the frequency difference between nearest-neighbor frequencies). At zero wavelength detuning, the analytic absolute threshold ($I_{\rm Simon}$) is reproduced. As $\Delta\omega \longrightarrow \infty$, the threshold goes to $N_\omega I_{\rm Simon}$ because the absolutely unstable modes become spatially decoupled (i.e., each frequency independently drives TPD at its own quarter-critical surface).

Figure 153.37(a) shows the spatial structure of the absolutely unstable plasma modes from an *LPSE* simulation of a monochromatic plane wave. The absolutely unstable modes occur over a narrow spatial region (~2 μm wide) centered at $x \approx 12\ \mu\text{m}\left(n_e/n_c = 0.244\right)$. Figure 153.37(b) shows the spatial structure of the absolute instability for $\Delta\omega/\omega_0 = 1\%$, where the absolutely unstable regions have separated spatially by ~4.1 μm. This corresponds to a 2% change in density, consistent with the expectation that the resonant density should vary as the square of the resonant frequency. Note that although the modes have separated spatially, the wavelength of the transverse beat between the unstable modes is shorter in the two-color case. Amplitude modulation in the pump beam causes the most-unstable transverse wave number to be larger (shorter wavelength) in the two-color case because of its square root dependence on the laser intensity.[9]

An unintuitive aspect of the results shown in Fig. 153.36 is that the instability threshold increases most rapidly in the two-color case at small $\Delta\omega$. Our expectation was that increasing the number of colors would increase the decoupling rate because the effective amount of temporal incoherence is an increasing function of N_ω. To verify that this is not an artifact of the time-enveloped pseudospectral solver used in *LPSE*, an independent test was performed by solving Eqs. (1) and (2) from Simon *et al.*,[9] which are not time enveloped, using finite differencing.

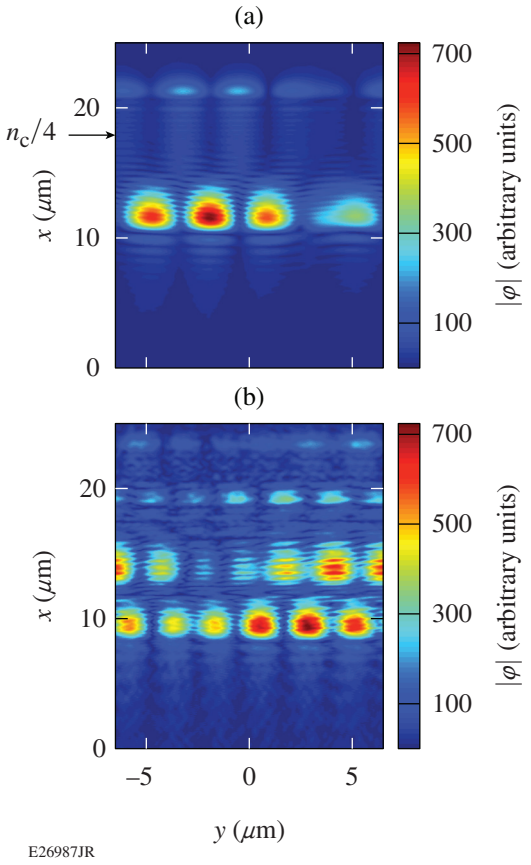

Figure 153.37
Color maps of the electrostatic potential from 2-D *LPSE* simulations late in time ($t = 10$ ps) when the field structure is dominated by the absolutely unstable modes. (a) Zero frequency detuning and (b) 1% frequency detuning (two color). Only a small portion of the simulation region is shown corresponding to $n_e/n_c = 0.23$ to 0.26.

The calculations were performed on a subscale grid, but the same qualitative behavior was observed. The large variation in threshold over the ensemble of initial phases for $N_\omega > 2$ suggests that amplitude modulation has a significant impact on the thresholds. When speckled beams are used, the threshold always increases with increasing N_ω, so this effect was not present in the 3-D calculations, all of which had speckled beams.

In summary, we have shown that hot-electron mitigation can potentially be achieved using the modest amount of laser frequency detuning that is available on existing laser facilities ($\Delta\omega/\omega_0 \sim 0.7\%$). Three-dimensional *LPSE* simulations using realistic direct-drive ICF conditions show that decoupling of the multibeam instability significantly increases the absolute instability threshold, and that suppression of the absolute instability effectively eliminates TPD-driven hot-electron generation. The validity of these results is supported by the fact that *LPSE* simulations have reproduced both wave-amplitude and hot-electron measurements from previous experiments. This method of TPD mitigation can be scaled to higher laser intensities by increasing the available frequency detuning, which can open up the design space for future ICF implosions.

ACKNOWLEDGMENT

This material is based upon work supported by the Department of Energy National Nuclear Security Administration under Award No. DE-NA0001944, the University of Rochester, and the New York State Energy Research and Development Authority. The support of the DOE does not constitute an endorsement by the DOE of the views expressed in this article.

REFERENCES

1. S. Atzeni and J. Meyer-ter-Vehn, *The Physics of Inertial Fusion: Beam Plasma Interaction, Hydrodynamics, Hot Dense Matter*, 1st ed., International Series of Monographs on Physics, Vol. 125 (Oxford University Press, Oxford, 2004).

2. R. S. Craxton, K. S. Anderson, T. R. Boehly, V. N. Goncharov, D. R. Harding, J. P. Knauer, R. L. McCrory, P. W. McKenty, D. D. Meyerhofer, J. F. Myatt, A. J. Schmitt, J. D. Sethian, R. W. Short, S. Skupsky, W. Theobald, W. L. Kruer, K. Tanaka, R. Betti, T. J. B. Collins, J. A. Delettrez, S. X. Hu, J. A. Marozas, A. V. Maximov, D. T. Michel, P. B. Radha, S. P. Regan, T. C. Sangster, W. Seka, A. A. Solodov, J. M. Soures, C. Stoeckl, and J. D. Zuegel, Phys. Plasmas **22**, 110501 (2015).

3. V. N. Goncharov, T. C. Sangster, R. Betti, T. R. Boehly, M. J. Bonino, T. J. B. Collins, R. S. Craxton, J. A. Delettrez, D. H. Edgell, R. Epstein, R. K. Follet, C. J. Forrest, D. H. Froula, V. Yu. Glebov, D. R. Harding, R. J. Henchen, S. X. Hu, I. V. Igumenshchev, R. Janezic, J. H. Kelly, T. J. Kessler, T. Z. Kosc, S. J. Loucks, J. A. Marozas, F. J. Marshall, A. V. Maximov, R. L. McCrory, P. W. McKenty, D. D. Meyerhofer, D. T. Michel, J. F. Myatt, R. Nora, P. B. Radha, S. P. Regan, W. Seka, W. T. Shmayda, R. W. Short, A. Shvydky, S. Skupsky, C. Stoeckl, B. Yaakobi, J. A. Frenje, M. Gatu-Johnson, R. D. Petrasso, and D. T. Casey, Phys. Plasmas **21**, 056315 (2014).

4. R. L. McCrory, D. D. Meyerhofer, R. Betti, R. S. Craxton, J. A. Delettrez, D. H. Edgell, V. Yu. Glebov, V. N. Goncharov, D. R. Harding, D. W. Jacobs-Perkins, J. P. Knauer, F. J. Marshall, P. W. McKenty, P. B. Radha, S. P. Regan, T. C. Sangster, W. Seka, R. W. Short, S. Skupsky, V. A. Smalyuk, J. M. Soures, C. Stoeckl, B. Yaakobi, D. Shvarts, J. A. Frenje, C. K. Li, R. D. Petrasso, and F. H. Séguin, Phys. Plasmas **15**, 055503 (2008).

5. T. R. Boehly, R. S. Craxton, T. H. Hinterman, J. H. Kelly, T. J. Kessler, S. A. Kumpan, S. A. Letzring, R. L. McCrory, S. F. B. Morse, W. Seka, S. Skupsky, J. M. Soures, and C. P. Verdon, Rev. Sci. Instrum. **66**, 508 (1995).

6. B. Yaakobi, C. Stoeckl, T. Boehly, D. D. Meyerhofer, and W. Seka, Phys. Plasmas **7**, 3714 (2000).

7. E. A. Jackson, Phys. Rev. **153**, 235 (1967).

8. C. S. Liu and M. N. Rosenbluth, Phys. Fluids **19**, 967 (1976).

9. A. Simon, R. W. Short, E. A. Williams, and T. Dewandre, Phys. Fluids **26**, 3107 (1983).

10. J. F. Myatt, J. Zhang, R. W. Short, A. V. Maximov, W. Seka, D. H. Froula, D. H. Edgell, D. T. Michel, I. V. Igumenshchev, D. E. Hinkel, P. Michel, and J. D. Moody, Phys. Plasmas **21**, 055501 (2014).

11. R. K. Follett, D. H. Edgell, R. J. Henchen, S. X. Hu, J. Katz, D. T. Michel, J. F. Myatt, J. Shaw, and D. H. Froula, Phys. Rev. E **91**, 031104(R) (2015).

12. W. Seka, D. H. Edgell, J. F. Myatt, A. V. Maximov, R. W. Short, V. N. Goncharov, and H. A. Baldis, Phys. Plasmas **16**, 052701 (2009).

13. R. Yan, C. Ren, J. Li, A. V. Maximov, W. B. Mori, Z.-M. Sheng, and F. S. Tsung, Phys. Rev. Lett. **108**, 175002 (2012).

14. D. H. Froula, I. V. Igumenshchev, D. T. Michel, D. H. Edgell, R. Follett, V. Yu. Glebov, V. N. Goncharov, J. Kwiatkowski, F. J. Marshall, P. B. Radha, W. Seka, C. Sorce, S. Stagnitto, C. Stoeckl, and T. C. Sangster, Phys. Rev. Lett. **108**, 125003 (2012).

15. B. Yaakobi, A. A. Solodov, J. F. Myatt, J. A. Delettrez, C. Stoeckl, and D. H. Froula, Phys. Plasmas **20**, 092706 (2013).

16. R. K. Follett, J. A. Delettrez, D. H. Edgell, V. N. Goncharov, R. J. Henchen, J. Katz, D. T. Michel, J. F. Myatt, J. Shaw, A. A. Solodov, C. Stoeckl, B. Yaakobi, and D. H. Froula, Phys. Rev. Lett. **116**, 155002 (2016).

17. J. F. Myatt, H. X. Vu, D. F. DuBois, D. A. Russell, J. Zhang, R. W. Short, and A. V. Maximov, Phys. Plasmas **20**, 052705 (2013).

18. C. Stoeckl, R. E. Bahr, B. Yaakobi, W. Seka, S. P. Regan, R. S. Craxton, J. A. Delettrez, R. W. Short, J. Myatt, A. V. Maximov, and H. Baldis, Phys. Rev. Lett. **90**, 235002 (2003).

19. D. F. DuBois, B. Bezzerides, and H. A. Rose, Phys. Fluids B **4**, 241 (1992).

20. D. T. Michel, A. V. Maximov, R. W. Short, S. X. Hu, J. F. Myatt, W. Seka, A. A. Solodov, B. Yaakobi, and D. H. Froula, Phys. Rev. Lett. **109**, 155007 (2012).

21. R. K. Follett, J. F. Myatt, J. G. Shaw, D. T. Michel, A. A. Solodov, D. H. Edgell, B. Yaakobi, and D. H. Froula, Phys. Plasmas **24**, 102134 (2017).

22. J. J. Thomson and J. I. Karush, Phys. Fluids **17**, 1608 (1974).

23. S. P. Obenschain *et al*., Phys. Rev. Lett. **56**, 2807 (1986).

24. P. Michel *et al*., Phys. Rev. Lett. **102**, 025004 (2009).

25. J. A. Marozas, M. Hohenberger, M. J. Rosenberg, D. Turnbull, T. J. B. Collins, P. B. Radha, P. W. McKenty, J. D. Zuegel, F. J. Marshall, S. P. Regan, T. C. Sangster, W. Seka, E. M. Campbell, V. N. Goncharov, M. W. Bowers, J.-M. G. DiNicola, G. Erbert, B. J. MacGowan, L. J. Pelz, and S. T. Yang, "First Observation of Cross-Beam Energy Transfer Mitigation for Direct-Drive Inertial Confinement Fusion Implosions Using Wavelength Detuning at the National Ignition Facility," to be published in Physical Review Letters.

26. G. Laval, R. Pellat, and D. Pesme, Phys. Rev. Lett. **36**, 192 (1976).

27. G. Laval *et al*., Phys. Fluids **20**, 2049 (1977).

28. D. Eimerl and A. J. Schmitt, Plasma Phys. Control. Fusion **58**, 115006 (2016).

29. Y. Zhao *et al*., Phys. Plasmas **24**, 112102 (2017).

30. J. Zhang, J. F. Myatt, R. W. Short, A. V. Maximov, H. X. Vu, D. F. DuBois, and D. A. Russell, Phys. Rev. Lett. **113**, 105001 (2014).

31. B. Fornberg, *A Practical Guide to Pseudospectral Methods*, Cambridge Monographs on Applied and Computational Mathematics, Vol. 1 (Cambridge University Press, Cambridge, England, 1998).

32. D. F. DuBois, D. A. Russell, and H. A. Rose, Phys. Rev. Lett. **74**, 3983 (1995).

33. J. Delettrez, R. Epstein, M. C. Richardson, P. A. Jaanimagi, and B. L. Henke, Phys. Rev. A **36**, 3926 (1987).

34. E. I. Moses *et al*., Phys. Plasmas **16**, 041006 (2009).

35. D. D. Meyerhofer, J. Bromage, C. Dorrer, J. H. Kelly, B. E. Kruschwitz, S. J. Loucks, R. L. McCrory, S. F. B. Morse, J. F. Myatt, P. M. Nilson, J. Qiao, T. C. Sangster, C. Stoeckl, L. J. Waxer, and J. D. Zuegel, J. Phys.: Conf. Ser. **244**, 032010 (2010).